J Mater Sci: Mater Electron (2016) 27:1738–1744
DOI 10.1007/s10854-015-3948-5

Effects of AlN buffer on the physical properties of GaN films grown on 6H-SiC substrates

Zhen Huang[1] · Yuantao Zhang[1] · Baijun Zhao[2] · Fan Yang[1] · Junyan Jiang[1] · Gaoqiang Deng[1] · Baozhu Li[1] · Hongwei Liang[3] · Yuchun Chang[1] · Junfeng Song[1]

Received: 20 July 2015 / Accepted: 22 October 2015 / Published online: 28 October 2015

Abstract In this study, 1.5-µm-thick GaN films with AlN buffer were prepared on 6H-SiC substrates by metal-organic chemical vapor deposition. To determine the effects of growth conditions of AlN buffer on crystalline quality and stress state of GaN films, two series of experiments were carried out. By optimizing growth conditions of AlN buffer, the full width at half maximum values of (0002) and $(10\bar{1}2)$ rocking curves of GaN films were improved to 136 and 225 arcsec, respectively. A smooth surface was obtained with a small root-mean-squared roughness of 0.332 nm and the excellent optical property was observed. Simultaneously, threading dislocation density and tensile stress in GaN films were reduced by increasing AlN buffer growth temperature and its thickness in some extent. Besides, stress values in GaN films were confirmed by Raman and low-temperature photoluminescence spectra, which indicated that the lower tensile stress in GaN film, the higher the film crystallinity.

✉ Yuantao Zhang
zhangyt@jlu.edu.cn

✉ Yuchun Chang
changyc@jlu.edu.cn

1 State Key Laboratory on Integrated Optoelectronics, College of Electronic Science and Engineering, Jilin University, Qianjin Street 2699, Changchun 130012, People's Republic of China

2 Changchun Institute of Applied Chemistry, Chinese Academy of Sciences, Changchun 130022, China

3 School of Physics and Optoelectronic Technology, Dalian University of Technology, Dalian 116024, China

1 Introduction

In recent years, research interests in III-nitride semiconductors have increased rapidly [1–3]. GaN-based high-speed, high-power electronic applications, especially for optoelectronic devices, such as blue and green light emitting diodes and laser diodes, have attracted considerable attentions due to their superior physical properties including wide direct energy band gap, strong chemical bonds, high breakdown electric field strength, and high thermal stability [4–6]. As we all known, high-quality GaN template is an important prerequisite for the fabrication of GaN-based electronic or optoelectronic devices. Meanwhile, the stress state in GaN films is a crucial influencing factor for device performance. Thus finding an effective method to improve the crystalline quality and the stress state in GaN films is especially important. Due to the lack of large-area GaN homogeneous epitaxial substrates, Al_2O_3, Si and 6H-SiC substrates are commonly used for the epitaxial growth of nitrides [7–9]. Among them, 6H-SiC has been proven as an appropriate substrate, due to its high thermal conductivity [4.9 W/(cm K)] and its small lattice mismatch with nitrides (for GaN about 3.3 %, and for AlN about 1 %) [10]. However, GaN films grow directly on 6H-SiC substrates, due to the large difference (about 33.1 %) of thermal expansion coefficients, produce substantial tensile stress during the cooling process [11]. Then, high density of cracks can be generated, especially when the films are thick. Consequently, in order to improve crystalline quality and reduce tensile stress in GaN films, AlN buffer is proposed due to the small lattice mismatch with 6H-SiC [12–14]. Meanwhile, the lattice constant a of AlN is larger than that of 6H-SiC, which means a compressive stress would be brought to neutralize the tensile stress generated during the cooling-down process. Therefore, the growth conditions of AlN buffer affect the properties of GaN films greatly. Koleske et al. [15] found that the electrical properties of GaN films were improved by increasing AlN growth temperature. Green et al. [16] showed that for the fabrication of high-performance AlGaN/GaN high electron mobility transistors, threading dislocations (TDs) in the upper GaN films were reduced by decreasing AlN buffer thickness, as a result leakage currents, trapping effects, and device reliability were significantly improved. Moe et al. [17] reported that AlN buffer grown at a high V/III ratio could improve the crystalline quality of subsequent GaN films. In above these literatures, the growth parameters of AlN buffer have been studied the effects on the crystalline quality and electrical properties of GaN films. However, there are few reports about the effects of AlN buffer on the stress state of GaN films, as well as the relationship between stress state and crystalline quality of GaN films. In this work, we investigate the effects of growth temperature and its thickness of AlN buffer on stress state of GaN films grown on 6H–SiC substrates. Meanwhile, the crystalline quality and optical properties of GaN films are also discussed.

2 Experimental procedures

GaN films were grown on 6H-SiC (0001) substrates by using AIXTRON CCS 3 × 2″ FT metal-organic chemical vapor deposition (MOCVD). Trimethylgallium (TMGa), trimethylaluminum (TMAl), and ammonia (NH_3) were used as Ga, Al, and N source precursors, respectively. Prior to the deposition, 6H-SiC substrates were heat-treated in an H_2 environment for 5 min at 1150 °C. Two series of samples, series I and II, were directly grown on 6H-SiC substrates. In series I, 100-nm-thick AlN buffer layers were deposited at different growth temperatures ranging from 1020 to 1140 °C with a TMAl flow rate of 19 μmol/min, and an NH_3 flow rate of 12 mmol/min. Then, 1.5-μm-thick GaN films were deposited at 1050 °C with a TMGa flow rate of 85 μmol/min, and an NH_3 flow rate of 134 mmol/min. In series II, AlN buffer layers with different growth thicknesses ranging from 60 to 200 nm were deposited using the optimized growth temperature, which was identified in series I, and then GaN films were deposited under the same growth conditions with series I.

The crystalline quality of GaN films was characterized by Rigaku X-ray diffraction (XRD). Optical properties were investigated by room-temperature photoluminescence (RT-PL) measurements, with a 325 nm He–Cd laser as the excitation source. In order to check the stress states of GaN films, Raman spectroscopy was measured by Renishaw Raman Microscope at room-temperature, with a 532 nm solid laser as the excitation source. Meanwhile, low-temperature photoluminescence (LT-PL) spectra were recorded at 13 K. Surface morphology of GaN film was examined by Veeco atomic force microscopy (AFM) equipment.

3 Results and discussions

During the growth process, EpiTT and EpiCurve in situ sensor systems are used to monitor and analyze the reflectance and curvature of the sample, respectively, as shown in Fig. 1. The surface flatness and the growth mode of the film are both evaluated based on the oscillation amplitude of the reflectance curve. Meanwhile, the combined effects of lattice and thermal expansion coefficient mismatch between the film and the substrate lead to individual wafer curvature. Figure 1a shows four distinct growth processes of GaN film grown on 6H-SiC substrate: heat treatment for 6H-SiC substrate, the growth of AlN buffer, the growth of GaN film, and cooling down the reactor. Reflectivity decreases rapidly during AlN growth due to the formation of AlN islands on 6H-SiC substrate. Moreover, reflectivity sinks to a rather low value during the initial stage of GaN growth, due to the production of GaN

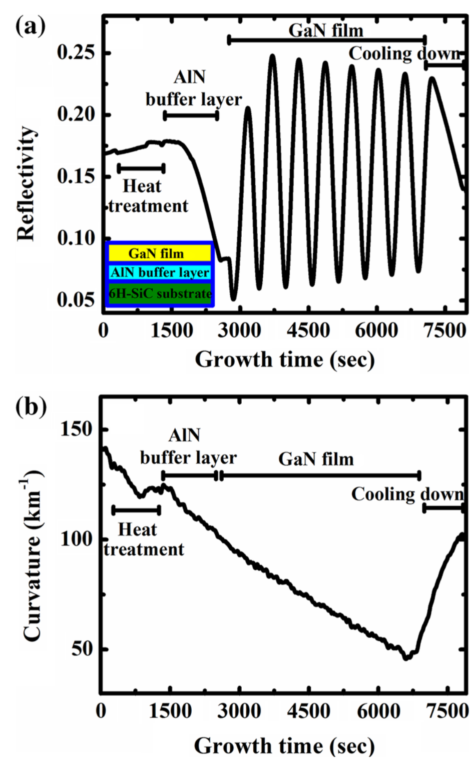

Fig. 1 In-situ test spectra of GaN film grown on SiC substrate at the optimized growth conditions of AlN buffer. **a** Optical reflectance *curve* using 950 nm by EpiTT measurement and **b** wafer curvature by Epicurve measurement

islands above the AlN buffer. As the growth continues, GaN film enters a two-dimensional (2D) growth mode, which is manifested by the stable oscillation amplitude of the reflectance curve. New uncoated wafers right out of the box usually have some curvature due to production tolerance. During the growth process, the curvature of wafer might be further changed. As shown in Fig. 1b, the initial curvature value is positive, which means the wafer is concave. As the growth continues, the curvature value gradually decreases, due to the existence of compressive stress in AlN buffer and GaN film. During the cooling-down process, tensile stress in GaN film increases gradually with the increase of the concave curvature, which could be attributed to the large thermal mismatch between GaN film and 6H-SiC substrate.

Figure 2 shows the dependences of the full width at half maximum (FWHM) values of X-ray omega-scan and dislocation densities of GaN films on AlN growth temperature (a) and buffer thickness (b). Furthermore, the FWHM values of (0002) rocking curve are associated with the density of screw dislocation, and that of $(10\bar{1}2)$ are related to the density of edge dislocation [18]. The dislocation density can be determined by the following equations [19]:

$$\rho_{screw} = \frac{\beta^2{}_{(0002)}}{2\pi \ln 2 \times b^2_{screw}} \tag{1}$$

$$\rho_{edge} = \frac{\beta^2{}_{(10\bar{1}2)}}{2\pi \ln 2 \times b^2_{edge}} \tag{2}$$

where ρ_{screw} and ρ_{edge} are the densities of screw and edge dislocations, $\beta_{(0002)}$ and $\beta_{(10\bar{1}2)}$ are the FWHM values of (0002) and $(10\bar{1}2)$ rocking curves, b_{screw} and b_{edge} are the Burgers vector of screw and edge dislocations, respectively. In series I, AlN growth temperatures were varied from 1020 to 1140 °C under the same thickness of 100 nm, as shown in Fig. 2a. The FWHM values of (0002) and $(10\bar{1}2)$ rocking curves reduce significantly to 136 and 225 arcsec from 284 and 402 arcsec, respectively, with increasing AlN growth temperatures from 1020 to 1080 °C. However, as the growth temperature further increases, it is found that the FWHM values of (0002) and $(10\bar{1}2)$ rocking curves both increase substantially to 245 and 325 arcsec, respectively. Therefore, the optimized AlN growth temperature of 1080 °C is obtained for the growth of GaN film. Meanwhile, the densities of both screw and edge dislocations reach a minimum of 3.7×10^7 cm^{-2} and 2.7×10^8 cm^{-2}, respectively. In series II, AlN thicknesses were changed from 60 to 200 nm under the optimal growth temperature of 1080 °C, as shown in Fig. 2b. As the AlN growth thicknesses increase from 60 to 100 nm, the FWHM values of (0002) and $(10\bar{1}2)$ rocking curves reduce substantially to 136 and 225 arcsec from 209 and

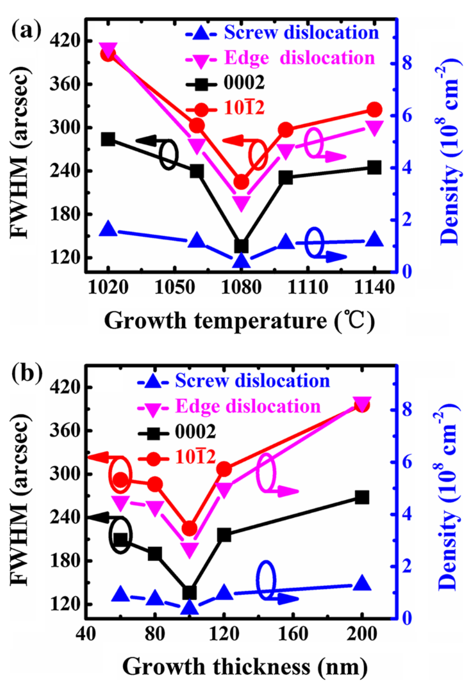

Fig. 2 Dependences of the FWHM values of X-ray omega-scan and dislocation densities of GaN films on AlN **a** growth temperatures and **b** its thicknesses

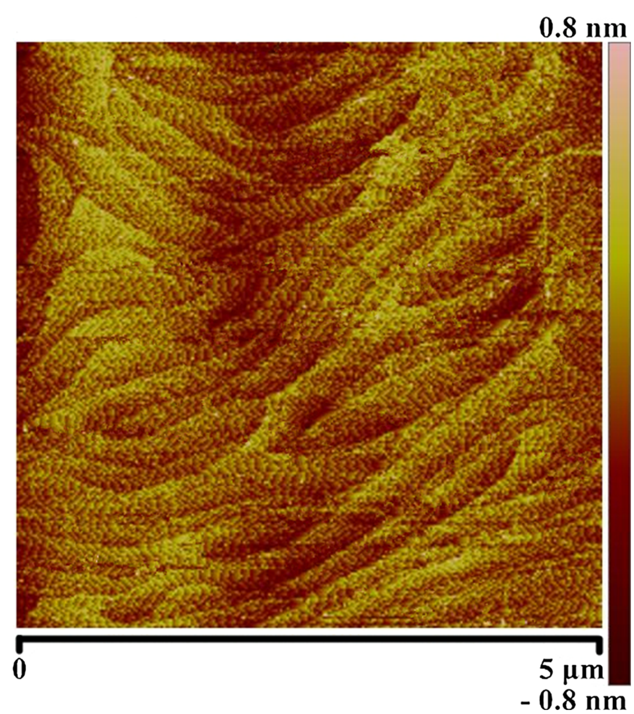

Fig. 3 Two-dimensional AFM surface morphology of GaN film prepared at the optimized growth conditions of AlN buffer with a scanning area of 5 × 5 μm^2

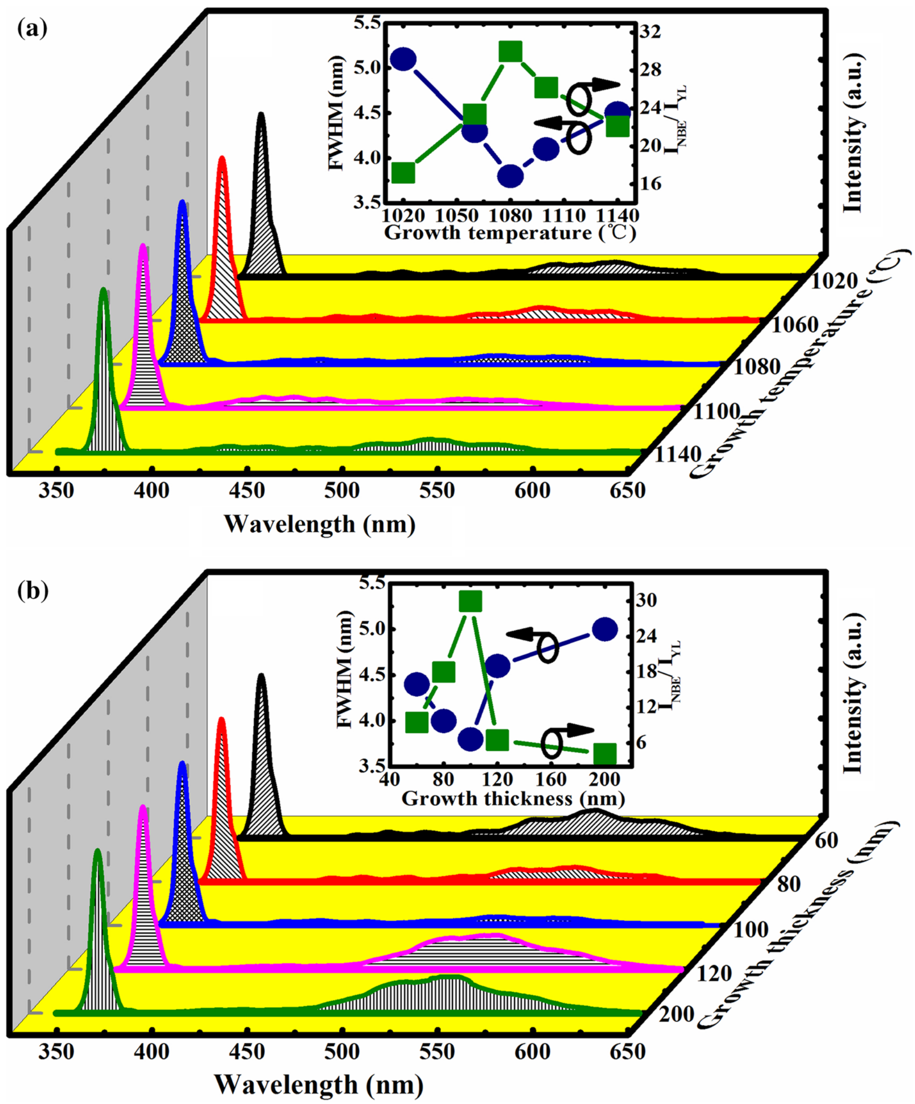

Fig. 4 RT-PL spectra of GaN films with different AlN **a** growth temperatures and **b** its thicknesses. The *insets* are the NBE FWHM values and the ratios of I_{NBE}/I_{YL} for GaN films

292 arcsec, respectively. However, as the thickness more increases, the FWHM values of (0002) and $(10\bar{1}2)$ rocking curves increase significantly to 268 and 396 arcsec, respectively. Therefore, the optimized AlN thickness of 100 nm is determined for the growth of GaN film. In conclusion, the above results indicate that the densities of both screw and edge dislocations can be reduced by changing AlN growth temperature and thickness in some extent. Figure 3 shows the AFM image of GaN film, with 100-nm-thick AlN buffer grown at 1080 °C, which indicates that the film was deposited in a step-flow growth mode. The roots mean-square value of the sample is 0.332 nm in $5 \times 5\ \mu m^2$ scanning area, which demonstrates a very smooth surface is obtained.

Figure 4 shows the RT-PL spectra of GaN films in series I (with different AlN buffer growth temperatures) and series II (with different AlN buffer thicknesses). For comparison, the spectra are normalized by the intensity of near-band-edge (NBE) emission peak. All GaN samples present excellent optical quality with dominant NBE emission at 365 nm and fairly weak yellow luminescence (YL) band emission around 550 nm. As shown in the inset of Fig. 4a, for the samples in series I, the ratio of I_{NBE}/I_{YL} increases regularly with the increase of AlN growth temperature from 1020 to 1080 °C, and then it begins to decrease gradually at buffer temperature higher than 1080 °C. While, for the FWHM values of NBE emissions, the opposite case is observed with the change of AlN growth temperature. The largest ratio and the smallest FWHM value are obtained for the GaN film with AlN buffer grown at 1080 °C, which means that film has the best optical quality in series I. Similarly, for the samples in series II shown in the inset of Fig. 4b, the ratios and the FWHM values show the same change tendency with series

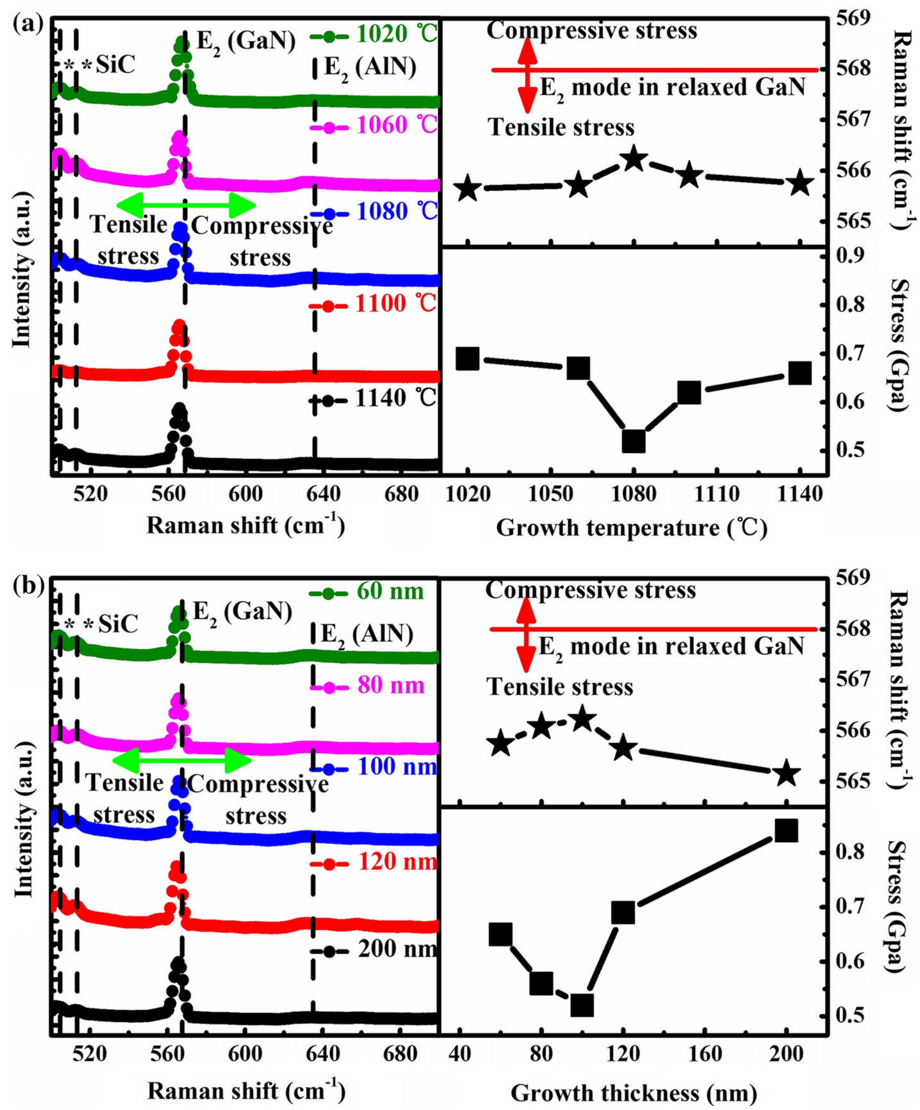

Fig. 5 Raman spectroscopy of GaN films with different AlN **a** growth temperatures and **b** its thicknesses

I, with the increase of AlN buffer thickness from 60 to 200 nm. For the GaN film with 100-nm-thick AlN buffer, the largest ratio and the smallest FWHM value are obtained, which indicates that the sample has a relatively good optical property in series II. Based on above discussions, it can be obtained that the GaN film with 100-nm-thick AlN buffer grown at 1080 °C has an optimal optical property. Optical properties of GaN films are well in accordance with the results of XRD performance in Fig. 2.

Furthermore, the stress states of GaN films are investigated by Raman spectroscopy and LT-PL spectra. The stress can be determined by the peak shift of E_2 (high) mode of GaN film in Raman spectroscopy [20]. Figure 5 shows Raman spectra near E_2 (high) modes of GaN films. In Fig. 5a, the peak positions of E_2 (high) modes for GaN films with different AlN growth temperatures are 565.65, 565.71, 566.23, 565.91, and 565.75 cm^{-1}, respectively. In Fig. 5b, the positions of E_2 modes for GaN films with different AlN thicknesses are 565.74, 566.09, 566.23, 565.66, and 565.16 cm^{-1}, respectively. In order to determine the stress state in GaN film, a reference peak position of 568.0 cm^{-1} is used for the stress-free GaN [21]. In comparison to the reference peak, an increase in E_2 (high) mode is due to compressive stress, whereas a decrease in E_2 (high) mode is ascribed to tensile stress. The stress σ is usually expressed in the following form [22]:

$$\Delta\omega = k\sigma \tag{3}$$

where $\Delta\omega$ is the peak shift (cm^{-1}), and k is the Raman stress factor. In series I, the calculated stress values in GaN films are 0.69, 0.67, 0.52, 0.62, and 0.66 GPa, respectively, as shown in Fig. 5a. In series II, the calculated stress values in GaN films are 0.65, 0.56, 0.52, 0.69, and 0.84 GPa, respectively, as shown in Fig. 5b. The results indicate the

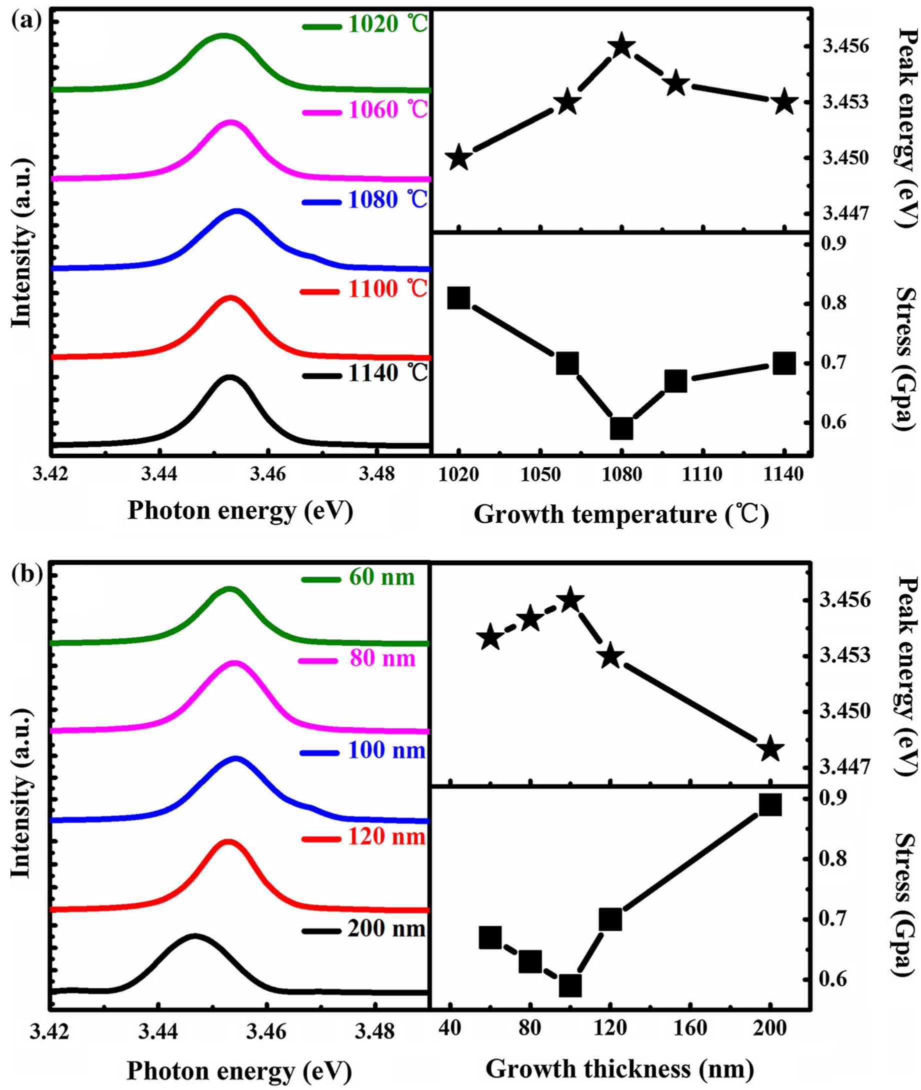

Fig. 6 LT-PL spectra of GaN films with different AlN **a** growth temperatures and **b** its thicknesses

presence of tensile stresses in all GaN films. Moreover, Taniyasu et al. [23] have confirmed that TDs can induce tensile stress, which increases with increasing TDs densities. It is in accordance with our results. The lower TDs densities exist in GaN films in Fig. 2, the lesser tensile stresses are obtained in Fig. 5.

Figure 6 shows the LT-PL spectra of GaN films at 13 K, the dominant emission peaks in which are related to the donor bound excitons (D^0X). The bandgap of a semiconductor may be affected by residual stress in the film. Tensile stress decreases the bandgap, while compressive stress increases the bandgap [24]. As shown in Fig. 6a, the D^0X peak positions of GaN films with different AlN growth temperatures are 3.450, 3.453, 3.456, 3.454, and 3.453 eV, respectively. As shown in Fig. 6b, the D^0X peak positions of GaN films with different AlN growth thickness are 3.454, 3.455, 3.456, 3.453, and 3.448 eV, respectively. The D^0X peak position for relaxed GaN is determined to be 3.472 eV [25]. The stress σ can be calculated using the following equation [26]:

$$\sigma = \Delta E/(-k) \tag{4}$$

where ΔE is the D^0X emission peak shift, and k is the stress factor. In series I, the calculated stress values in GaN films are 0.81, 0.70, 0.59, 0.67, and 0.70 GPa, respectively, as shown in Fig. 6a. In series II, the calculated stress values in GaN films are 0.67, 0.63, 0.59, 0.70, and 0.89 GPa, respectively, as shown in Fig. 6b. The change trend of stress values is same with that of Raman results shown in Fig. 5, which confirms our conclusions further.

4 Conclusions

In summary, two series experiments have been carried out to optimize the physical properties of GaN films with AlN buffer on 6H-SiC substrates. At the optimized AlN growth temperature of 1080 °C and its thickness of 100 nm, the crystallinity, the optical property, and the stress state of the upper GaN film could be tuned to achieve the best results. The typical FWHM values of (0002) and $(10\bar{1}2)$ rocking curves of GaN films were 136 and 225 arcsec, respectively. The optical property of GaN film was remarkable in terms of a rather large I_{NBE}/I_{YL} and reduced FWHM value of NBE emission. By analysing Raman and LT-PL spectra, we found that all GaN samples were at the status of tensile stress and the residual strains in the films could be effectively suppressed by increasing AlN buffer growth temperature and its thickness in some extent. The same changing trend of physical properties of GaN films in two series of experiments demonstrated that the lower tensile stress in GaN film, the higher the film's crystalline quality. It is reasonably believed that our results presented here will aid design and development of reliable GaN-based electronic or optoelectronic devices.

Acknowledgments This work was supported by the National Natural Science Foundation of China (Nos. 61106003, 61274023, 61223005 and 61376046), the Science and Technology Developing Project of Jilin Province (20130204032GX and 20150519004JH), and the Program for New Century Excellent Talents in University (NCET-13-0254).

References

1. X.T. Liu, D.B. Li, X.J. Sun, Z.M. Li, H. Song, H. Jiang, Y.R. Chen, CrystEngComm **16**, 8058 (2014)
2. O. Hironori, K. Tsunenobu, S. Jun, Appl. Phys. Lett. **105**, 071603 (2014)
3. D. Won, J.M. Redwing, J. Cryst. Growth **377**, 51 (2013)
4. D.S. Wang, H.W. Liang, P.C. Tao, K.X. Zhang, S.W. Song, Y. Liu, X.C. Xia, R.S. Shen, G.T. Du, Superlattices Microstruct. **70**, 54 (2014)
5. R.R. Sumathi, P. Gille, J. Mater. Sci. Mater. Electron. **25**, 3733 (2014)
6. S. Kitagawa, H. Miyake, K. Hiramatsu, J. Appl. Phys. **53**, 05FL03 (2014)
7. L. Zhang, J.X. Yu, X.P. Hao, Y.Z. Wu, Y.B. Dai, Y.L. Shao, H.D. Zhang, Y. Tian, Sci. Rep. **4**, 4179 (2014)
8. P.C. Tao, H.W. Liang, X.C. Xia, Q.J. Feng, D.S. Wang, Y. Liu, R.S. Shen, K.X. Zhang, X. Cai, Y.M. Luo, G.T. Du, J. Mater. Sci. Mater. Electron. **25**, 4268 (2014)
9. Z.F. Shi, Y.T. Zhang, B. Wu, X.P. Cai, J.X. Zhang, X.C. Xia, H. Wang, X. Dong, H.W. Liang, B.L. Zhang, G.T. Du, Appl. Phys. Lett. **102**, 161101 (2013)
10. E. Cho, A. Mogilatenko, F. Brunner, E. Richter, M. Weyers, J. Cryst. Growth **371**, 45 (2013)
11. G.J. Ding, L.W. Guo, Z.G. Xing, Y. Chen, P.Q. Xu, H.Q. Jia, J.M. Zhou, H. Chen, J. Semicond. **31**, 033003 (2010)
12. K. Mitsuaki, O. Hironori, I. Ryota, F. Mitsuru, K. Yoichi, K. Tsunenobu, S. Jun, Appl. Phys. Express **6**, 062604 (2013)
13. S.W. Song, Y. Liu, H.W. Liang, D.C. Yang, K.X. Zhang, X.C. Xia, R.S. Shen, G.T. Du, J. Mater. Sci. Mater. Electron. **24**, 2923 (2013)
14. Y.X. Cui, Y.M. Wang, C. Wen, B.H. Ge, F.H. Li, Y. Chen, H. Chen, Ultramicroscopy **126**, 77 (2013)
15. D.D. Koleske, R.L. Henry, M.E. Twigg, J.C. Culbertson, S.C. Binari, A.E. Wickenden, M. Fatemi, Appl. Phys. Lett. **80**, 4372 (2002)
16. D.S. Green, S.R. Gibb, B. Hosse, R. Vetury, D.E. Grider, J.A. Smart, J. Cryst. Growth **272**, 285 (2004)
17. C.G. Moe, Y. Wu, S. Keller, J.S. Speck, S.P. DenBaars, D. Emerson, Phys. Status Solidi A **203**, 1708 (2006)
18. D.C. Yang, H.W. Liang, Y. Qiu, S.W. Song, Y. Liu, R.S. Shen, Y.M. Luo, G.T. Du, J. Mater. Sci. Mater. Electron. **24**, 2716 (2013)
19. Y.R. Chen, H. Song, D.B. Li, X.J. Sun, H. Jiang, Z.M. Li, G.Q. Miao, Z.W. Zhang, Y. Zhou, Mater. Lett. **114**, 26 (2014)
20. S. Qu, S.Q. Li, Y. Peng, X.L. Zhu, X.B. Hu, C.X. Wang, X.F. Chen, Y.Q. Gao, X.G. Xu, J. Alloys Compd. **502**, 417 (2010)
21. D.G. Zhao, S.J. Xu, M.H. Xie, S.Y. Tong, H. Yang, Appl. Phys. Lett. **83**, 677 (2003)
22. J.M. Wagner, F. Bechstedt, Appl. Phys. Lett. **77**, 346 (2000)
23. Y. Taniyasu, M. Kasu, T. Makimoto, J. Cryst. Growth **298**, 310 (2007)
24. I. Ahmad, M. Holtz, N.N. Faleev, H. Temkin, J. Appl. Phys. **95**, 1692 (2004)
25. H. Siegle, A. Hoffmann, L. Eckey, C. Thomsen, J. Christen, F. Bertram, D. Schmidt, D. Rudloff, K. Hiramatsu, Appl. Phys. Lett. **71**, 2490 (1997)
26. J.C. Zhang, D.G. Zhao, J.F. Wang, Y.T. Wang, J. Chen, J.P. Liu, H. Yang, J. Cryst. Growth **268**, 24 (2004)